IEEE Access
Multidisciplinary ⋮ Rapid Review ⋮ Open Access Journal

Received 14 April 2025, accepted 14 May 2025, date of publication 19 May 2025, date of current version 28 May 2025.

Digital Object Identifier 10.1109/ACCESS.2025.3571610

RESEARCH ARTICLE

A Comprehensive Methodology of Field-Oriented Control Design With Parameter Variation Analysis for Interior Permanent Magnet Synchronous Machine Drives

TIAGO DAVI CURI BUSARELLO[1], (Senior Member, IEEE), ABDULLAH BUBSHAIT[2], ORUGANTI V. S. R. VARAPRASAD[3], (Member, IEEE), ABDULHAKEEM ALSALEEM[4], AND MARCELO GODOY SIMÕES[5], (Fellow, IEEE)
[1]Department of Control, Automation and Computation Engineering, Federal University of Santa Catarina, Florianopolis 88040-900, Brazil
[2]Department of Electrical Engineering, College of Engineering, King Faisal University, Al Ahsa 31982, Saudi Arabia
[3]Smart Transportation Electrification and Energy Research (STEER) Group, Department of Electrical, Computer, and Software Engineering, Faculty of Engineering and Applied Science, Ontario Tech University, Oshawa, ON L1G 0C5, Canada
[4]Department of Electrical Engineering, College of Engineering, Qassim University, Buraydah 52571, Saudi Arabia
[5]School of Technology and Innovations, University of Vaasa, 65200 Vaasa, Finland

Corresponding author: Tiago Davi Curi Busarello (tiago.busarello@ufsc.br)

This work was supported by the Coordination for the Improvement of Higher Education Personnel–Coordenação de Aperfeiçoamento de Pessoal de Nível Superior (CAPES) through the Article Processing Charge (ROR identifier: 00xma614).

ABSTRACT This paper proposes a comprehensive methodology for Field-Oriented Control (FOC) with parameter variation analysis for Interior Permanent Magnet Synchronous Machines (IPMSM). The modeling approach for an IPMSM is first presented, followed by a step-by-step procedure for designing a vector-controlled strategy. The formulation is based on a *dq*-rotating reference frame aligned with the rotor shaft position. A key distinction of this methodology from traditional approaches is that the current controller is designed in the time domain based on desired time constants, while the speed control is formulated within a frequency response domain framework. The proposed hybrid approach enables accurate tuning of the Proportional-Integrator (PI) controllers for both current and speed control loops. Additionally, a parameter variation analysis is conducted to enhance the proposed methodology. The validity region for the design procedure is presented, ensuring that for any wide speed variation of the machine, loop gains are properly tuned. One of the main advantages of the proposed methodology is that it provides a fast, reliable, and accurate technique for implementing IPMSM drive systems. Results from a Controller Hardware-in-the-Loop (C-HIL) setup with an external microcontroller are presented. The comprehensive design approach is validated under two different IPMSM parameter sets, demonstrating its effectiveness.

INDEX TERMS Electric machines, controller hardware-in-the-loop, vector control, permanent magnet machines, variable speed drives.

I. INTRODUCTION

The Permanent Magnet Synchronous Machine (PMSM) drive is a mature technology widely used in engineering applications. In recent years, PMSMs have gained considerable attention due to their increasing adoption in the electric vehicle sector, primarily because of their high power density, low maintenance, and excellent controllability. PMSMs are typically constructed with either surface-mounted or interior magnets, with the latter being more suitable for high-speed applications. In such cases, the machine is referred to as an Interior Permanent Magnet Synchronous Machine (IPMSM).

The associate editor coordinating the review of this manuscript and approving it for publication was Qiang Li.

A key characteristic of these machines is that the quadrature and direct inductances are equal in surface-mounted PMSMs but differ in interior-mounted configurations [1].

Regardless of magnet placement, PMSM speed and position must be accurately controlled. While PMSM control strategies are well established in the literature, the growing use of PMSMs in electric vehicles has introduced new challenges for industry and academia. One such challenge is the development of a design methodology that accommodates a wide range of operating speeds while considering parameter variations.

A. LITERATURE REVIEW

Two of the most common control strategies for IPMSMs are Field-Oriented Control (FOC) and Direct Torque Control (DTC). The FOC approach regulates stator current in a rotating reference frame while controlling the IPMSM speed. The reference frame can be aligned with the stator flux, rotor flux, or other variables. By measuring the stator current and transforming it from the *abc* reference frame to *dq* coordinates using the rotor flux frame, the d-axis and q-axis currents can be controlled independently. In this configuration, i_q represents the torque-producing current, while i_d corresponds to the flux-producing current. The speed controller's output serves as the reference for the q-axis, while the d-axis reference is typically set to zero to minimize reluctance torque.

In the FOC strategy, rotor position must be determined using either a resolver or observer techniques [2], [3], [4]. The *dq*-axis current and speed control loops are typically implemented using Proportional-Integral (PI) controllers [5], requiring three PI controllers in total. It is worth noting that in FOC, the *dq*-axes are inherently coupled.

There is extensive literature on PI controller tuning for FOC-based PMSM strategies, with various approaches aimed at enhancing performance [6], [7], [8], [9], [10], [11], [12], [13], [14], [15], [16]. For instance, [6] introduces a novel space vector pulse-width modulation scheme in which the space vector plane is redivided, and the coordinates of the nearest three vectors and their duty cycles are determined by locating the reference vector. The optimal switching state and sequence are selected online to minimize switching losses while maintaining low common-mode voltage. However, the complexity of this method may limit its practical implementation.

A comparative analysis of DTC and FOC for PMSMs is presented in [7], demonstrating the effectiveness of both control strategies. However, the study omits details on PI controller tuning. Meanwhile, [8] examines a fail-operational FOC approach but serves more as a case study than a rigorous design methodology. Similarly, [9] proposes a user interface for PMSM drive control, with limited emphasis on controller design and without validation of reference signal tracking.

A switched system theory combined with FOC for PMSM is explored in [17]. While attractive for handling parameter variations, this approach complicates the FOC design process. A lower-complexity FOC strategy aiming to decouple the *dq*-axes is introduced in [18], utilizing a zero-pole placement technique. However, selecting appropriate zero and pole locations is nontrivial and requires significant expertise.

FOC is a well-established and reliable method for IPMSM control [19], [20], [21], [22], [23], [24], [25]. Conventional FOC employs a cascaded closed-loop structure, with an outer loop tracking a predefined speed and an inner loop regulating the *dq*-axis currents to generate voltage references. Practical applications often encounter perturbations in electrical and mechanical parameters, such as stator inductance, permanent magnet flux linkage, and moment of inertia, due to factors like magnetic saturation, temperature variations, demagnetization, aging, and load torque changes [26], [27], [28], [29], [30].

These disturbances can cause undesired transients and fluctuations, affecting control performance and potentially compromising the power conversion system's integrity. Consequently, improving the robustness of conventional control algorithms is crucial. Various advanced control methods have been explored, including Model Predictive Control (MPC) [21], [31], [32], Active Disturbance Rejection Control (ADRC) [33], self-tuning control [34], u-synthesis control [35], sliding mode control (SMC) [25], [36], [37], Model-less Adaptive Control with Recursive Least Squares (MARS) [38], and deadbeat-based controllers [39].

Each of these methods has trade-offs. For instance, while MPC optimizes control actions over a finite prediction horizon and considers constraints, its computational complexity can introduce delays in real-time applications. ADRC and self-tuning controllers adapt control laws dynamically, while SMC, despite its robustness, may cause chattering and introduce high-frequency harmonics requiring additional filtering. MARS offers model-independent adaptation but may have slower convergence and higher computational demands [40].

For current-controlled IPMSM drives, the PI controller remains the preferred choice due to its simplicity, robustness, and reliability. However, there is a need for improved tuning methodologies to enhance response times while maintaining the advantages of conventional PI control.

Most state-of-the-art methodologies focus on inner-loop current control for specific PMSM configurations, often neglecting systematic tuning of the outer speed control loop. Consequently, *ad-hoc* trial-and-error tuning is commonly employed. This paper addresses this gap by proposing a rigorous, step-by-step procedure for designing a closed-loop speed controller for FOC, ensuring robustness and mathematical precision.

B. NOVELTIES AND GOALS

This paper presents a comprehensive design approach for FOC-based IPMSM control. While extensive literature exists on tuning PI controllers for the *dq*-axis, there is a notable

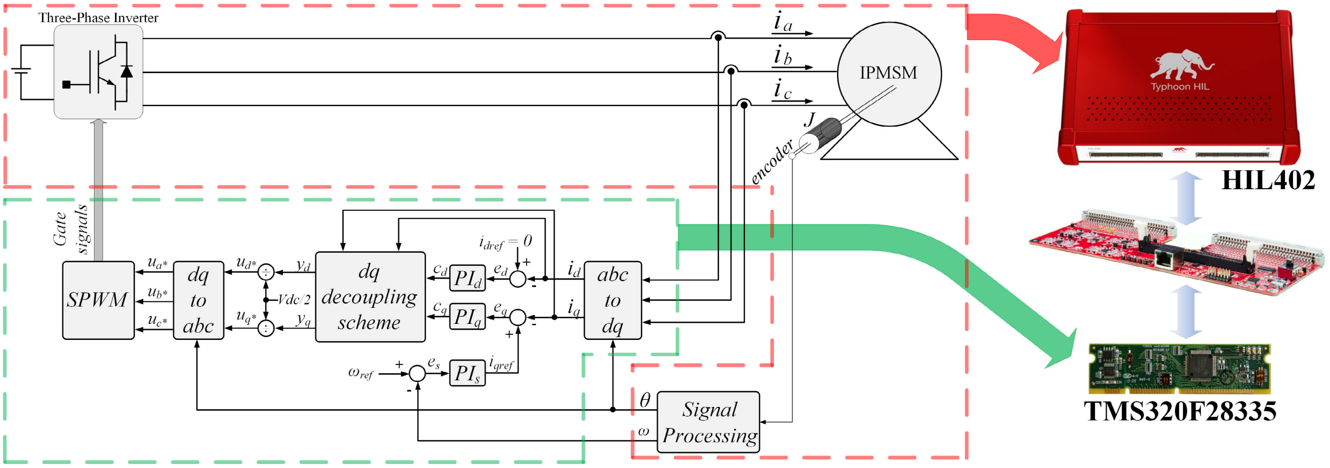

FIGURE 1. Simplified diagram of the PMSM drive system and its control strategy.

gap in frequency response-based design methodologies for speed control. To the best of the author's knowledge, no previous work has systematically applied a frequency response approach to the outer speed control loop. Although several papers propose advanced control strategies, none adopt this methodology.

Since PI controllers are inherently linear, this paper also defines an operational region in which the designed controllers achieve satisfactory performance in terms of torque and speed. Such analysis is rarely found in the literature.

A step-by-step procedure for tuning the PI controllers in an IPMSM drive based on the FOC strategy is provided, ensuring proper system performance. The proposed approach is validated using a Hardware-in-the-Loop (HIL) setup with an external microcontroller. Specifically, the IPMSM and inverter are simulated within a Typhoon HIL 402, while the control strategy runs on a TMS320F28335 microcontroller. Initial findings of this research can be found in [41]. The key contributions of this paper are as follows:

- Proposing an enhanced step-by-step FOC design approach that is more straightforward than existing methods.
- Introducing a parameter variation analysis to improve FOC accuracy.
- Designing the speed controller using a frequency response methodology.
- Defining the boundaries of validity for the proposed design approach, given the linear nature of the controllers and wide PMSM speed variations.
- Demonstrating that the methodology is applicable to both IPMSMs and surface-mounted PMSMs by setting $L_d = L_q = L_s$.

II. SYSTEM DESCRIPTION

Fig. 1 presents a simplified diagram of the IPMSM drive system. The system has a DC source, which may come from a front-end rectifier, a three-phase inverter, and the IPMSM. The phases A, B, and C of the stator current (i_a, i_b, i_c) are measured and sent to the control strategy block. The measurement of stator current for phase C could be eliminated, and its value could be computed within the microcontroller. Similarly, the machine electrical speed (ω) and the electric rotor angle (θ) are also obtained using position and speed transducers. These variables could be estimated with observers [42]. The measured signals are sent to the control strategy block, which in turn produces the gate signals for the transistors of the inverter. The figure also highlights how the parts of the system were verified experimentally in the C-HIL setup.

The control strategy block diagram of FOC is also presented in Fig. 1. The three-phase stator current is converted to dq-rotating reference frame. The d-axis current is compared with zero, and the resulting signal is sent to the PI controller (PI_d). Note that this comparison is not necessary, but it is kept here for the sake of clarity. For q-axis current, the comparison is with the output signal of the PI controller of the speed loop (PI_s). Then, the resulting signal is sent to the PI controller (PI_q) of the q-axis. The PI controllers will later be referred to as $G_{iq}(s)$ and $G_{id}(s)$. At the end, the dq-axis signals are converted back to abc-reference frame, and their output is modulated using Space Vector Pulse-Width Modulator (SVPWM). L_d and L_q are the direct- and quadrature-axis inductances, respectively. λ is the flux linkage of the rotor magnets. V_{dc} is the value in volts of the DC source. After the PI controllers of the dq-axis, there is a dq decoupling scheme and the inverter gain compensation. The dq decoupling scheme consists of adding and subtracting terms to the output signal of the current controllers. Such terms are dependent on the dq currents, the stator inductances, and the angular speed.

III. DYNAMIC MODEL FOR IPMSM

Before presenting the step-by-step procedure of tuning the PIs for the FOC strategy, it is convenient to present the equations that describe the dynamic behavior of the

IPMSM. The equations are in the rotor-reference frame. Some assumptions for IPMSM modeling are: the stator windings of the machine are distributed sinusoidally; the flux density around the machine air gap is sinusoidal; the machine is supplied by a converter system with no switching harmonics; core and stray losses are ignored; and the machine has sinusoidal induced EMF.

As briefly mentioned in the introduction, there are different types of PMSMs depending on the configuration and the placement of their magnets. The design of the machine determines its intrinsic parameter values. In surface-mounted PMSMs, the difference between the quadrature-axis and direct-axis inductances is very small, and they can be considered equal when modeling the PMSM. On the other hand, in IPMSMs, the ratio between the inductances of the quadrature and direct axes is typically 2 to 3. In this case, the modeling should consider such inductances as different parameters.

A. DYNAMIC ELECTRIC MODEL FOR IPMSM

The IPMSM dynamic behavior is described by the following equations:

$$v_q = R_s i_q + L_q \frac{di_q}{dt} + \omega_r L_d i_d + \omega_r \lambda_{af} \tag{1}$$

$$v_d = R_s i_d + L_d \frac{di_d}{dt} - \omega_r L_q i_q \tag{2}$$

where v_q and v_d are the stator voltage for q and d axis, i_q and i_d are the stator current for q and d axis, R_s is the stator resistance, L_q and L_d are the inductance for q and d axis, ω_r is the electrical speed, λ_{af} is the air gap flux linkage.

Defining two new variables as:

$$u_q = -\omega_r L_d i_d - \omega_r \lambda_{af} + v_q \tag{3}$$

$$u_d = \omega_r L_d i_d + v_d \tag{4}$$

These equations are used in the dq decoupling scheme of Fig. 1 Therefore, the output variable of such scheme for d and q axis are given respectively by.

$$y_q = c_q + \omega_r L_d i_d + \omega_r \lambda_{af} \tag{5}$$

$$y_d = c_d - \omega_r L_q i_q \tag{6}$$

Since the decoupling scheme results in dq axis totally uncoupled, (1) and (2) can be written as the following equations.

$$u_q = R_s i_q + L_q \frac{di_q}{dt} \tag{7}$$

$$u_d = R_s i_d + L_d \frac{di_d}{dt} \tag{8}$$

As a result of that, the previous equations represent two decoupled subsystems and two independent controllers can be employed to make the i_d and i_q follow their reference signals. Taking the Laplace transformation of (7) and (8) and arranging them, one can get (9) and (10). These equations are the system's plant for the current control meshes.

$$G_{id}(s) = \frac{K_s}{1 + s\tau_d} \tag{9}$$

$$G_{iq}(s) = \frac{K_s}{1 + s\tau_q} \tag{10}$$

where,

$$K_s = 1/R_s;\ \tau_d = \frac{L_d}{R_s};\ \tau_q = \frac{L_q}{R_s} \tag{11}$$

where K_s is a static gain.

The abc to dq conversion is obtained through two parts using (12) and (13). For dq to abc their inverted matrices are used.

$$\begin{bmatrix} i_\alpha \\ i_\beta \end{bmatrix} = \begin{bmatrix} \frac{2}{3} & \frac{-1}{3} & \frac{-1}{3} \\ 0 & \frac{1}{\sqrt{3}} & \frac{-1}{\sqrt{3}} \end{bmatrix} \begin{bmatrix} i_a \\ i_b \\ i_c \end{bmatrix} \tag{12}$$

$$\begin{bmatrix} i_d \\ i_q \end{bmatrix} = \begin{bmatrix} sin(\theta) & -cos(\theta) \\ cos(\theta) & sin(\theta) \end{bmatrix} \begin{bmatrix} i_\alpha \\ i_\beta \end{bmatrix} \tag{13}$$

B. DYNAMIC MECHANICAL MODEL FOR IPMSM

The electromechanical torque is given by:

$$T_e = \frac{3}{2}\frac{P}{2}(\lambda_{af} i_q + (L_d - Lq) i_d i_q) \tag{14}$$

where P is the number of poles. For $i_{ds=0}$, (14) results in:

$$T_e = \frac{3}{2}\frac{P}{2}\lambda_{af} i_q \tag{15}$$

The electrical torque can also be written as:

$$T_e = K_{te} i_{qs} \tag{16}$$

where

$$K_{te} = \frac{3}{4} P \lambda_{af} \tag{17}$$

C. PARAMETER VARIATION OF IPMSM

Current and speed controllers are designed using variables such as flux linkage, stator resistance, and quadrature- and direct-axis inductances of the machine. These parameters may deviate from their nominal values depending on the operating conditions, as they are sensitive to saturation, magnet temperature, and aging. High temperatures affect the stator resistance and the flux linkage of the machine, whereas saturation can affect the inductances.

In the literature, researchers have explored various methods for parameter estimation in Permanent Magnet Synchronous Motors (PMSMs), which can be categorized into two main groups: offline and online approaches. Offline methods involve conducting dedicated tests where input/output data is collected with the motor disconnected from its application. These tests cover the entire torque-speed range, providing the data required for parameter estimation and generating look-up tables for control purposes. Although finite element analysis (FEA) offers an alternative to laboratory tests, both methods have limitations.

Laboratory tests are costly and time-consuming, while FEA may introduce inaccuracies due to modeling complexities and manufacturing imperfections [43], [44], [45].

On the other hand, online methodologies estimate parameters during normal on-load operations through real-time techniques implemented on the drive control unit. These approaches commonly utilize numerical methods, state observers, and artificial intelligence techniques [46], [47]. However, they face a challenge known as the rank-deficiency issue, where the number of unknown parameters exceeds the rank of the PMSM model, leading to inaccurate and simultaneous parameter estimations. One solution to this challenge involves reducing the number of unknown parameters by assuming some to have nominal values. However, retrieving these nominal values is not always feasible, and achieving convergence to actual values is not guaranteed. Operating conditions, aging effects, and incipient faults can further widen the gap between nominal and actual values, negatively impacting estimation accuracy. More advanced but expensive alternatives include using additional measurements, such as torque meters. Another option is signal injection [48] (current, voltage, or rotor position offset) to increase the system's rank. However, maintaining high signal-to-noise ratios is critical for accurate estimations without influencing machine parameters.

It is worth noting that the inductances on the direct axis (L_d) and quadrature axis (L_q) significantly depend on the i_d and i_q currents, temperature, rotor angle, and load angle. The model complexity is kept manageable to ensure practicality by considering only the current dependencies during machine control, as they have the most significant impact. As a reasonable assumption, changes in stator resistance (R_s), stator currents of the direct axis (i_d) and quadrature axis (i_q), L_d, and L_q are expected to be within $\pm 10\%$ of their actual values.

The quadrature-axis inductance is more sensitive to saturation than the direct-axis inductance. For instance, the stator resistance of the IPMSM can reach twice its nominal value, and the flux linkage of the rotor may drop to about 20% of its maximum value. The self-inductance of the quadrature-axis may fluctuate between 0.8 and 1.1 times its nominal value [1]. Therefore, the system plants presented in (9) and (10) are not stationary. Varying quadrature-axis inductance or stator resistance will impact the dynamic response of the system.

1) INFLUENCE OF PARAMETER VARIATION

In a PMSM, the dq-axis inductances are determined by the rotor shape. In addition, the q-axis induction is affected by the area between the air gap and magnet, called the pole piece, and the area between the N and S magnetic poles, called the web. The inductance term L_x varies during the machine operation due to magnetic saturation. If ΔL_x is a percentage of change in inductance, its actual value is written as:

$$L'_x = (1 + \Delta L_x)L_x \tag{18}$$

where x represents the axis, either d or q and L'_x is the actual inductance.

Therefore, the following equations describe the changes in the PMSM parameters due to their variation.

$$L'_d = (1 + \Delta L_d)L_d \tag{19}$$
$$L'_q = (1 + \Delta L_q)L_q \tag{20}$$
$$R'_s = (1 + \Delta R_s)R_s \tag{21}$$
$$\delta' = (1 + \Delta\delta)\delta \tag{22}$$
$$i'_{ds} = (1 + \Delta i_d s)i_d s \tag{23}$$
$$i'_{qs} = (1 + \Delta i_q s)i_q s \tag{24}$$

The parameter changes described in equations (19) to (24) are replaced by their original variables in the IPMSM dynamic model, as defined in equations (1) to (8). By performing these substitutions, the influence of the IPMSM parameters on the current and speed controllers can be evaluated, as will be demonstrated in Section V.

2) IMPACT OF INDUCTANCE VARIATIONS ON LOSSES OF IPMSM

In the IPMSM, copper losses are the resistance losses that occur in the stator windings. Assuming The copper losses is given by:

$$P_{cu} = 3i_s^2R_s \tag{25}$$

Taking ΔP_{cu} term as the amount of change, the copper loss expression is given as:

$$(1 + \Delta P_{cu})P_{cu} = 3(1 + \Delta i_s)i_s^2R_s \tag{26}$$

D. FLUX WEAKENING CONTROL

This section discusses flux-weakening control and explains why it is not employed in this paper. The aim of this paper is to design a controller that allows the IPMSM to follow a certain desired reference speed. The original idea was to demonstrate the performance of the controller below and at the rated speed. The maximum (rated) speed of the IPMSM is constrained by the stator input voltage, which is limited by the DC-link voltage. In some applications, such as electric vehicles, it is desirable to exceed the maximum speed of the machine.

To increase the speed of the IPMSM above its rated speed, the flux-weakening approach can be enabled. There are several methods to implement this approach. One common method is to calculate the dq-axes current references directly from the torque [49], [50]. This method does not directly impact the design process adapted in this paper.

Flux-weakening can be incorporated into the control loop of a classical FOC strategy, as shown in Fig. 2. For normal operation, the dq-axes currents can be calculated using the model equations. On the other hand, the d-axis current can be reduced (made negative) to decrease the flux of the IPMSM. The dq-axes current references are then used to feed the designed current controllers.

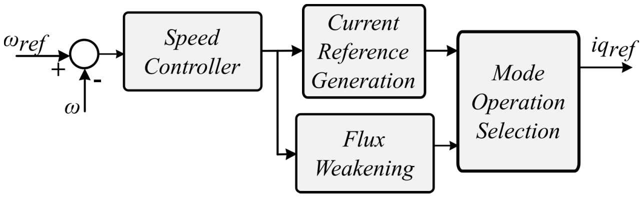

FIGURE 2. Inclusion of flux weakening control in FOC strategy.

Another reason for not employing flux-weakening control in the proposed FOC strategy is that flux-weakening operation is useful when the application needs to exceed the rated speed of the machine, reaching ultra-high speeds. Therefore, it is typically beneficial for transportation applications, where a significant amount of torque is initially required to accelerate a car, locomotive, or surface train, and then, at already high speeds, it may still need to move slightly further. In industrial and commercial applications, however, flux-weakening is not often applicable.

IV. STEP-BY-STEP PROCEDURE

The main purpose of proposing a comprehensive and clear methodology for designing the PI controllers of the FOC strategy is to provide an accurate and straightforward method. The intention is not to develop a control strategy superior to the advanced and nonlinear control strategies for PMSM drive applications commonly found in the literature, but rather to establish a better and clearer methodology for designing the PI controllers of FOC, particularly the PI controller for the speed control loop. The following step-by-step procedure is proposed to facilitate the design process and to present the entire procedure of designing the FOC strategy in a comprehensive manner. A comparison of speed response superiority with a common method is provided, and the results are shown in the Appendix.

The step-by-step procedure for designing the PIs of the FOC strategy is divided into two parts: one for the current controller and another for the speed controller, as follows.

A. CURRENT CONTROLLER

Fig. 3 presents a simplified control strategy block diagram for designing the current controllers. Note that such a simplified diagram is valid due to the decoupling scheme. Moreover, the simplified diagram is intended to enable the use of the proposed methodology for designing the PIs of the FOC strategy.

The C_{iq} and C_{id} are the PI controllers and given respectively by:

$$C_{iq}(s) = \frac{k_{pq}s + k_{iq}}{s} \tag{27}$$

$$C_{id}(s) = \frac{k_{pd}s + k_{id}}{s} \tag{28}$$

1st step: knowing the system parameters: The first step in designing the FOC strategy for IPMSM is to know the system parameters. Tab. 1 shows the parameters and their unit that must be known.

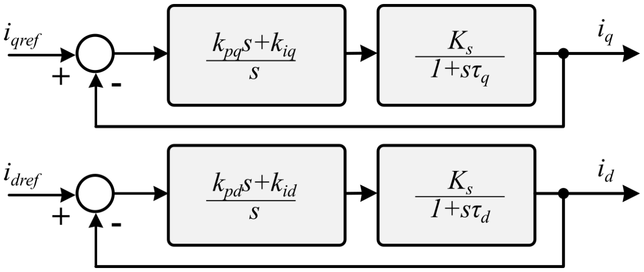

FIGURE 3. Simplified control strategy block diagram for designing the current controllers.

TABLE 1. Parameters and their units.

Parameters	Unit
Stator Resistance (R_s)	Ω
Direct inductance (L_q)	H
Quadrature inductance (L_q)	H
Number of Poles (P)	–
Flux linkage (λ)	Wb
Moment of inertia (J)	$k_g m^2$
Rotating damper (B)	$Nm/(rad/s)$
Inverter switching frequency (f_{sw})	Hz

2nd step: defining the desired time constant for the current controllers: The second step is to define the desired closed-loop time constant for the current controllers. Such a time constant is defined as τ and its unis is seconds. τ should be small for a fast response but large enough because $1/\tau$ is the bandwidth of the closed-loop system. However, $1/\tau$ must be at least 10 times lower than switching frequency (in rad/s) of the inverter. The time constant is usually chosen in the range of 0.5 ms to 2 ms. The time constants for the dq-axis are given as;

$$\tau = \tau_{iq} = \tau_{id} \tag{29}$$

3rd step: computing the proportional gain of the q-axis PI controller: The proportional gain of the q-axis PI controller is given by:

$$k_{pq} = \frac{L_q}{\tau_{iq}} \tag{30}$$

4th step: computing the integral gain of the q-axis PI controller: The integral gain of the q-axis PI controller is given by:

$$k_{iq} = \frac{R_s}{\tau_{iq}} \tag{31}$$

By using these values for kp and Ki, a pole-zero cancellation happens and the open loop transfer function will be a simple integrator that has a gain of zero dB at the cutoff frequency that corresponds to the chosen time constant.

5th step: computing the proportional gain of the d-axis PI controller: The proportional gain of the d-axis PI controller is given by:

$$k_{pd} = \frac{L_d}{\tau_{id}} \tag{32}$$

6th step: computing the integral gain of the d-axis PI controller: The integral gain of the d-axis PI controller is given by (33). Notice tha this gain is the same for the q-axis.

$$k_{id} = \frac{R_s}{\tau_{id}} \tag{33}$$

To define the time constant of the PIs for the q- and d-axis, one may compute $\frac{k_{pq}}{k_{iq}}$ and $\frac{k_{pd}}{k_{id}}$, respectively.

B. SPEED CONTROLLER

Fig. 4 presents the control strategy block diagram for designing the speed controller. The internal current control closed loop $\frac{i_q(s)}{I_{qref}(s)}$ and can be considered as unitary since the time constant of the speed control mesh is at least ten times larger than that for the current control mesh.

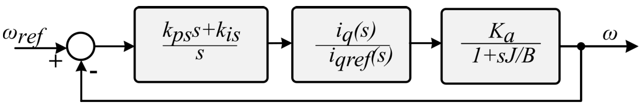

FIGURE 4. Control strategy block diagram for designing the speed controller.

The speed controller $C_s(s)$ is given by:

$$C_s(s) = \frac{k_{ps}s + k_{is}}{s} \tag{34}$$

The speed system plant G_s is given by:

$$G_s(s) = \frac{K_a}{1 + s\frac{J}{B}} \tag{35}$$

where K_a is given by:

$$K_a = \frac{0.75P\lambda}{B} \tag{36}$$

1st step: defining the desired time constant for the speed controller: The first step in designing the speed controller is to define the desired time constant. In order to make the inter and outer loop decoupled and the inner loop as unitary, the time constant for the speed controller must be at least ten times higher than the time constant of the current control mesh. Therefore, the time constant is defined in this paper as:

$$\tau_s = 10\tau_{iq} \tag{37}$$

2nd step: defining the curt-off frequency (f_c) of the closed-loop speed controller: The second step is to define a cut-off frequency for the closed-loop speed control. A rule of thumb from the control system theory says that the cut-off frequency of an outer loop must be ten times lower than the cut-off frequency of an inner loop. By doing that, the inner and outer loop has no coupling effects, and they can be designed individually. In this paper, the cut-off frequency is chosen as $1/\tau$, in Hz.

3rd step: computing the proportional gain of the speed controller: The proportional gain of the speed controller is computed through the open-loop frequency response of the speed system plant. By plotting such a frequency response and with a well defined cut-off frequency, one may pick how much is the gain a the desired cut-off frequency. Fig. 5 presents an example of how to compute the gain supposing in which the desired cut-off frequency is $200\,Hz$. G_{dB} is the gain at the desired cut-off frequency.

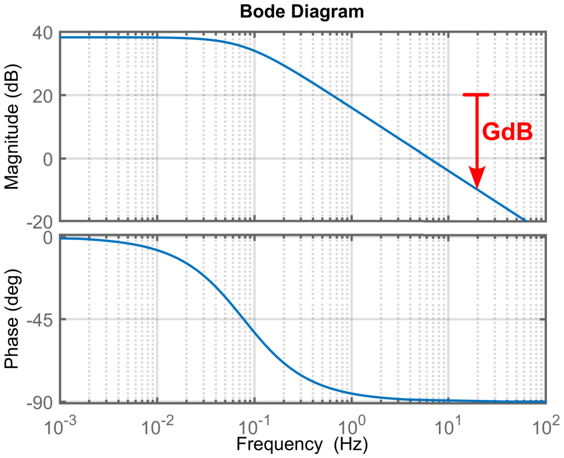

FIGURE 5. An example of how to compute the gain supposing that the desired cut-off frequency is $200\,Hz$.

The proportional gain of the speed controller is then given by (38). Note that the absolute value of G_{dB} is used in the equation.

$$k_{ps} = 10^{\frac{|G_{dB}|}{20}} \tag{38}$$

4th step: computing the integral gain of the speed controller: The fourth step, the last one, is computing the integral gain of the speed controller. It is given by:

$$k_{is} = \frac{k_{ps}}{\tau_s} \tag{39}$$

Fig. 6 presents a flowchart summarizing the steps for designing the current and speed control loops. Notice that after computing all coefficients of the PI controllers there is a process of performing parameter variation and stability analyses. This process is important to guarantee that the designed PIs are sufficient for making the IPMSM to work consistently in a desired region of operation. Such analyses are presented in Sections V and VI. The flowchart shows that if the analyses show unsatisfactory behavior, the designer can choose different time-constants and redesign the PI controllers.

V. INFLUENCE OF PARAMETER VARIATION IN THE CONTROLLERS

The control design procedure was based on the nominal values of the IPMSM. In this section, the sensitivity to parameter variations on the system dynamics and control

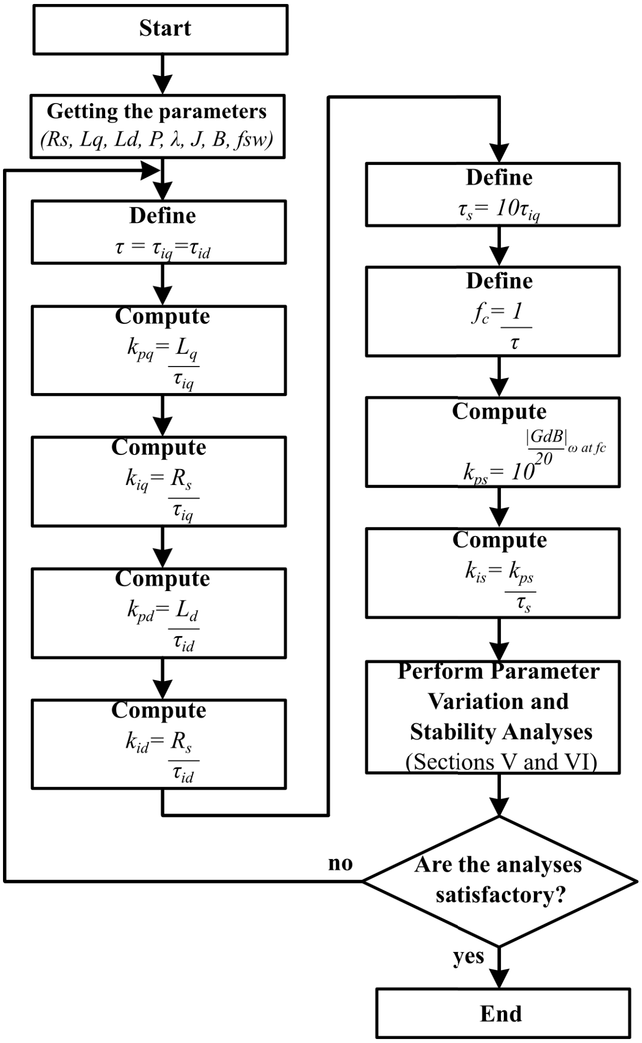

FIGURE 6. Flowchart summarizing the steps for designing the current and speed control loops.

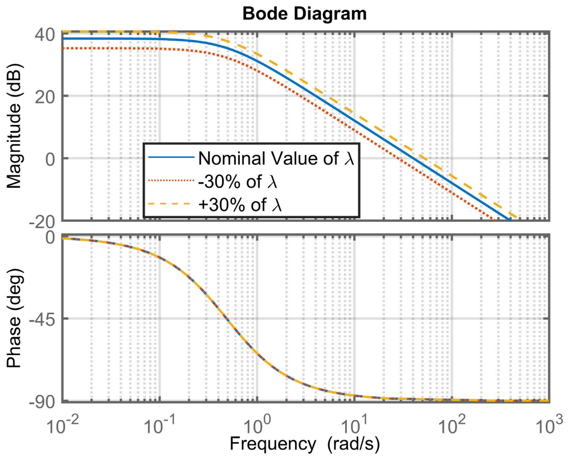

FIGURE 7. Frequency response of the mechanical system pant G(s) for different flux linkages.

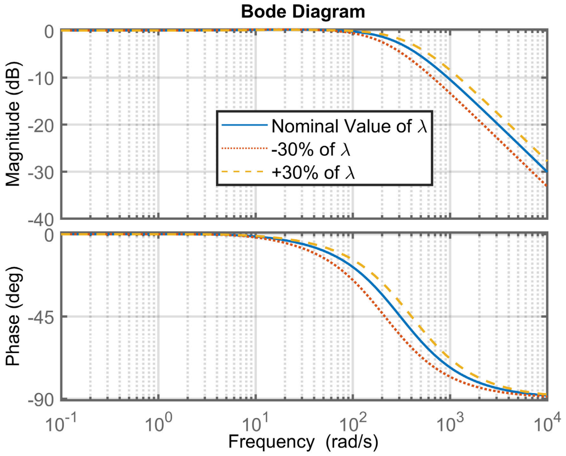

FIGURE 8. Frequency response of the closed loop of the speed system for different flux linkages.

design will be discussed. Hereinafter, all the bode plots and zero-pole map are generated using the parameters listed in Table 2. Consequently, the analysis of parameter variation is based on the initial values provided in Table 2.

First, the response of the mechanical system to flux linkage deviation is analyzed. The speed controller is designed based on the nominal values of the machine. The system plant is analyzed assuming a drop in the flux linkage by 30% and an increase in the flux linkage by 30%. Fig. 7 shows the frequency response of the uncompensated mechanical system, $G_s(s)$, for the nominal value of flux linkage, -30%, and $+30\%$.

Fig. 8 shows the response of the compensated system for all three values. It can be noticed that the variation of the flux linkage has almost zero impact on the performance of the controller.

Second, the response of q-axis current system is analyzed for variation in the quadrature inductance values due to saturation effect. The response of the q-axis loop is studied for two different values of L_q. Fig. 9 shows the response of the compensated system for all three values while Fig. 10 shows the time response of the compensated system for all three values.

Fig. 11 provides a comprehensive view of how key control and performance parameters in a PMSM system respond to variations in motor electrical characteristics and design choices. Fig. 11a depicts the relationship between the proportional gain k_{pd}, the direct-axis inductance L_d, and the current control time constant τ. The chart shows that k_{pd} increases with both L_d and τ, although the relationship becomes nonlinear for higher values of L_d. In Fig. 11b, the speed loop proportional gain k_{ps} is mapped against the magnetic flux linkage λ and the viscous friction coefficient B. This plot highlights the sensitivity of k_{ps} to the flux linkage, particularly in low-friction scenarios, emphasizing the impact of demagnetization on speed control performance. Fig. 11c shows copper losses as a function of the stator resistance variation ΔR_s and the relative current deviation δ_{is}. The

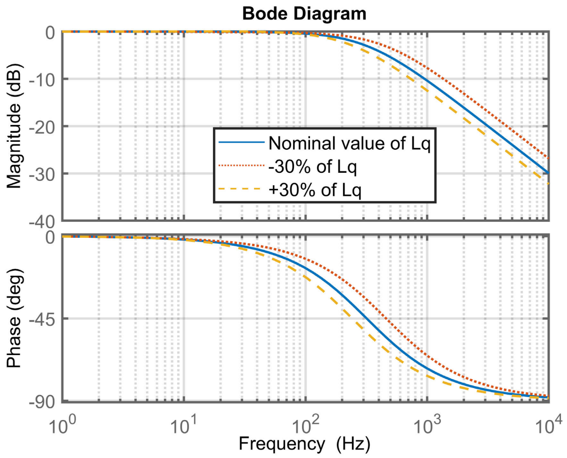

FIGURE 9. Frequency response of the closed loop of the q-axis for different L_q.

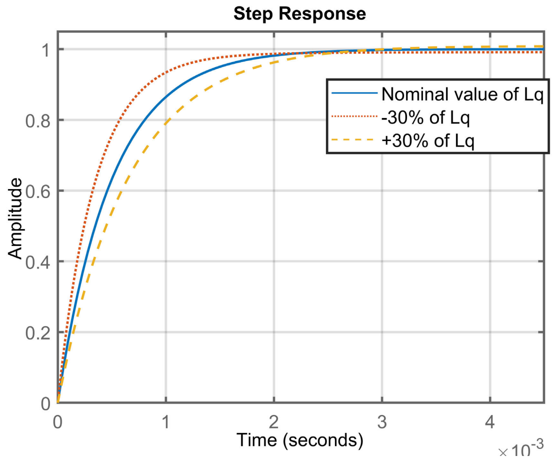

FIGURE 10. Time response of the closed loop of the q-axis for different L_q.

chart clearly shows that copper losses grow significantly with both increases in resistance and current, illustrating the compounding thermal effects that can arise in faulty or degraded conditions.

In Fig. 11d, it explores how the current control time constant τ_q varies with stator resistance R_s and quadrature-axis inductance L_q. The response surface indicates that higher L_q values help mitigate the adverse effects of increased resistance on dynamic response time. Fig. 11e continues the analysis by showing how the proportional gain k_{pq} of the q-axis current controller changes with R_s and L_q. The result reveals a nearly linear inverse relationship between k_{pq} and resistance, while a direct relationship exists with inductance, guiding the tuning strategy under parametric shifts. Lastly, Fig. 11f illustrates the torque sensitivity coefficient k_s as a function of R_s and L_q. It demonstrates that k_s degrades steeply with increased resistance, especially when L_q is low, reinforcing the critical role of accurate resistance estimation for torque control. Together, these plots offer valuable insights into the robustness of control parameters against parameter uncertainties.

VI. STABILITY AND REGION OF OPERATION

After finding the control loop parameters, the closed loop transfer function is given by (40)

$$G_{CL} = \frac{G_s(s)C_s(s)}{1+G_s(s)C_s(s)} = \frac{K_{ps}s + K_{is}}{\frac{J}{K_aB}s^2 + (K_{ps} + \frac{1}{K_a})s + K_{is}} \tag{40}$$

Using the parameters of the Table 2 and the proposed methodology shown in the previous section, it results in (41)

$$G_{CL} = \frac{7.9062s + 59.75}{0.02516s^2 + 7.9185s + 59.75} \tag{41}$$

TABLE 2. System parameter for evaluating the stability region of operation.

Parameters	Value
V_{dc}	$500\,V$
R_s	$1.3\,\Omega$
L_q	$17.2\,mH$
L_d	$8.9\,mH$
P	6
λ	$0.1819\,Wb$
J	$0.0206\,k_gm^2$
B	0.01
f_{sw}	$10\,kHz$

By plotting the pole-zero map of the closed-loop transfer function, as seen in Fig. 12, the stability of the system can be determined:

All the system's poles reside on the left-hand plane, which indicates that the system is stable. After validating the stability of the closed-loop system, the controller's performance can then be tested to define the region of operation and how it reacts to the physical limitations of the system. Since the controller's design approach produces specific control parameters, i.e., K_{ps} and K_{is}, a comprehensive test is conducted to determine how well the controller operates under different conditions.

The PI controllers used in the FOC strategy are linear in nature. They are tuned considering one point of operation. However, the designed PI controllers can operate satisfactorily within a region of operation. The parameters from Tab. 3 were used to obtain the region of operation.

The designed FOC strategy has been tested with different speed setpoints using Typhoon HIL software. In addition, the controller was tested under different loading conditions, with a load torque range from 2.5 Nm to 12.5 Nm and a speed range from 30 rad/s to 510 rad/s. It has been observed that the controller yielded zero steady-state error and a stable step-change response within the region of operation, as shown in Fig. 13.

The speed control range decreases as the load torque increases. When the motor operates under a relatively higher load, the step response range to the speed reference variation becomes narrower. Alternatively, higher speed ranges can be achieved under lower load torques.

The main purpose of the higher time constant is to make the speed control loop view the inner control loop as a unity

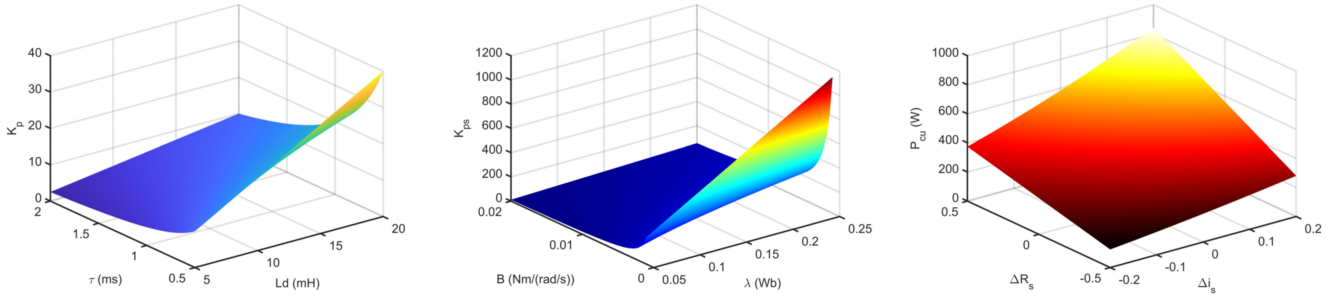

(a) k_{pd} vs L_d vs τ (b) k_{ps} vs λ vs B (c) Copper Loss vs δ_{is} vs Δ_{Rs}

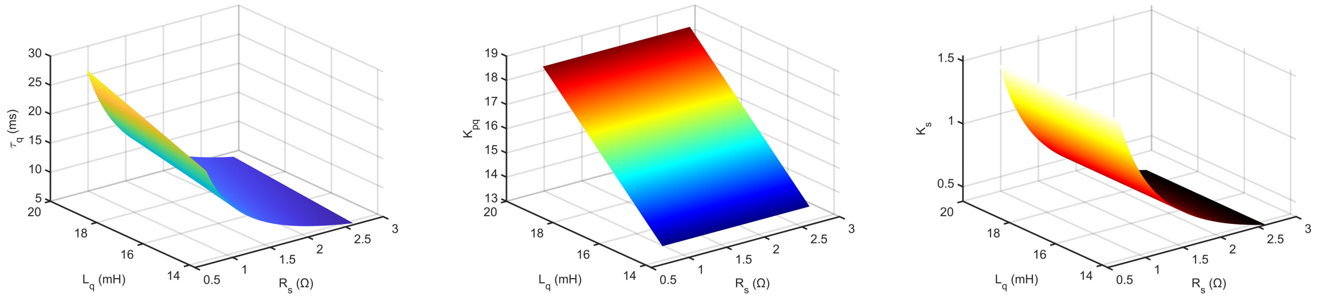

(d) τ_q vs R_s and L_q e) k_{pq} vs R_s vs L_q (f) k_s vs R_s vs L_q

FIGURE 11. **Comprehensive view of how key control and performance parameters in a PMSM system respond to variations in motor electrical characteristics and design choices.**

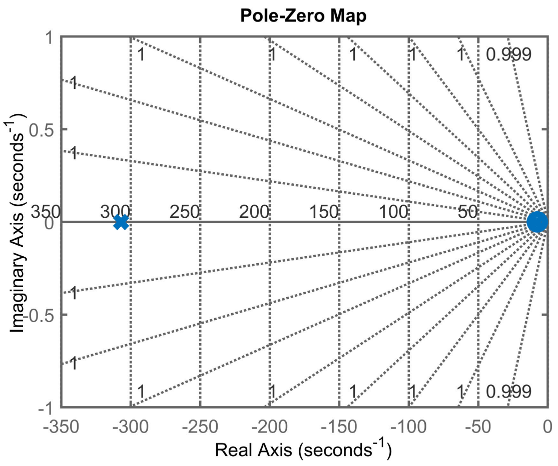

FIGURE 12. **Pole-Zero map of the closed-loop transfer function.**

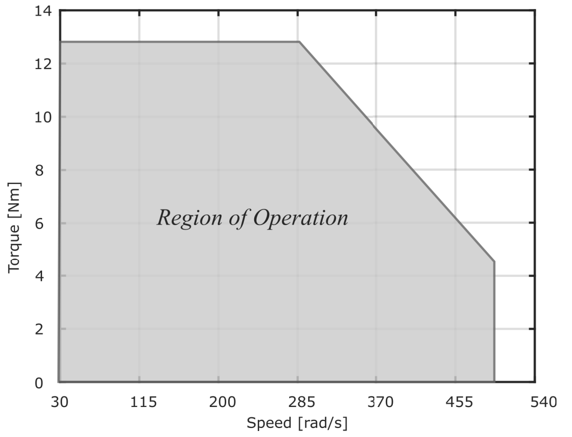

FIGURE 13. **Region of operation for the specified K_p and K_i designed for the speed control considering the parameters shown in Tab. 3.**

gain, and the time constant is not large enough to affect the response of the speed loop. The time response of the speed loop control, even with parameter variation, remains in the millisecond range, which is acceptable for the speed loop.

From (40), a change in the stator resistance of the machine would affect the parameters K_s and τ_d. As long as the factors of the characteristic equation remain greater than zero, e.g., $\frac{\tau_d}{K_s} > 0$, $K_{pd} + \frac{1}{K_s} > 0$, and $K_{id} > 0$, the system remains stable. However, the time response of the controller would differ slightly. Figs. 14 and 15 show, respectively, the system gain changes when the stator resistance is increased by around 33% and its step response for the same K_{pd} and K_{id}.

Since the purpose of incorporating changes in the stator resistance and inductance is to improve the control loop of the machine, the time response can be observed to identify variations in the stator resistance and inductance. By adapting the changes in K_{pd} and K_{id} to match the rate of change in the stator resistance and inductance, the time response of the system can be maintained.

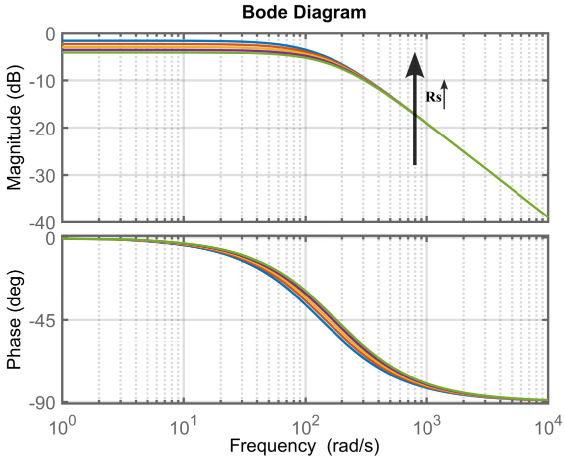

FIGURE 14. System gain changes if the stator resistance is increased to around 33%.

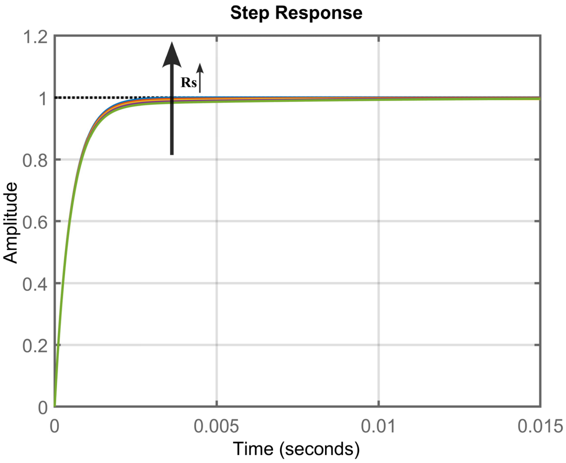

FIGURE 15. Step response for the designed K_{pd} and K_{id} if the stator resistance is increased to around 33%.

Changes in the stator resistance only affect K_{id} and K_{iq}, while changes in the inductance only affect K_{pd} and K_{pq}. The decoupling allows for an independent sweep of K_p and K_i to identify variations in either the stator resistance or inductance.

Therefore, a set of K_p and K_i values can be varied to produce a constant time response and identify changes in either the stator resistance or inductance. Fig. 16 shows the range and trajectory of K_p and K_i values for a specific range of changes in both the stator resistance and inductance, with respect to a constant time response.

VII. CONTROLLER HARDWARE-IN-THE-LOOP RESULTS

Two case studies were conducted in order to verify the proposed comprehensive design approach of FOC for IPMSM. Both of them were tested on C-HIL with external microcontroller. The real-time simulator is the Typhoon HIL402 while the microcontroller is the Texas Instruments TMS320F28335. The IPMSM, the inverter and sensors run on HIL402. The FOC strategy shown in Fig. 1 runs whiting the microcontroller. The red and green dashed boxes shown in such a figure better illustrates the aforementioned statements. In Appendix, there are a simulation results showing the controlled variables following their reference signals.

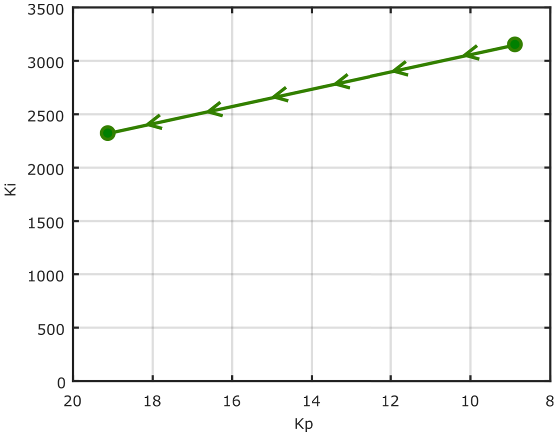

FIGURE 16. Range and trajectory of K_p and K_i to produce a constant time response for a 30% range of change in the stator resistance and a 50% range of change in the stator inductance.

Verification of a research in a C-HIL setup has some legitimacy because the control strategy runs in a real physical device. Since the power plant is properly modeled in the real-time simulator, and such simulator has very low latency, the microcontroller may not distinguish whether its interaction is with a real system or with a system which is being emulated in the real-time simulator. For researches that the focus is on a control strategy, an optimization algorithm or a decision-taker algorithm, the C-HIL setup appears as an interesting solution for experimental verification. Since the main focus of this paper is the FOC strategy, and due to laboratory resources, a C-HIL setup was used.

The following results present variables of different natures and units, such as Amperes, RPM, angle, and torque. Since all channels display signals in Volts, it's important to clarify the following: (i) for speed measurements, the indication of 2000 RPM per Volt means that the motor runs at 2000 RPM for every 1 V shown on the curve, regardless of the voltage-per-division setting selected on the oscilloscope. (ii) the same applies to current and torque measurements, with their respective scaling factors. (iii) For angle measurements, a scaling factor of 20 units per Volt is used, meaning that one Volt corresponds to 2π radians, as configured in the encoder.

A. FIRST CASE

Tab. 2 shows the parameter of the first case evaluated on C-HIL and microcontroller. The desired parameters are $\tau = 0.5\,ms$ and $f_c = 200\,Hz$. After following the step-by-step procedure for current and speed controllers, the FOC is fully designed. Tab. 2 also presents the designed parameters. For digital implementation of the FOC strategy into the microcontroller, the Backward Euler method was used to discretize the PI controllers.

TABLE 3. System parameter for Case 1.

Parameters	Value
R_s	$1.3\,\Omega$
V_{dc}	$500\,V$
L_q	$17.2\,mH$
L_d	$8.9\,mH$
P	6
λ	$0.1819\,Wb$
J	$0.0206\,k_g m^2$
B	0.01
k_{pq}	34.39999
k_{iq}	2600
k_{pd}	17.8000
k_{id}	2600
k_{ps}	7.906283
k_{is}	59.756796
f_{sw}	$10\,kHz$

Fig. 17 presents the electrical speed (ω), the stator current for phases a and b (i_a, i_b) and the electrical rotor position (θ) for steady-state operation. In this case, the reference speed is 2000 RPM and the load torque is 10 Nm.

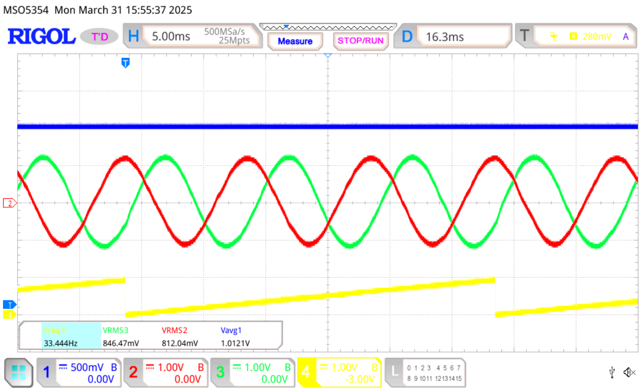

FIGURE 17. The electrical speed (ω) in channel 1, the stator current for phases a and b (i_a, i_b) in channels 2 and 3 and the electrical rotor position (θ) in channel 4 for steady-state operation. Ch1:2000RPM/V Ch2:Ch3: 10A/V; Ch4: 20 units/V.

Fig. 18 presents the electrical speed (ω), the stator current for phases a and b (i_a, i_b) and the mechanical load torque (T_L) for a transition of the load torque from 10 Nm to 2.5 Nm. The electrical speed oscillates and returns to its nominal value after some seconds, indicating that speed controller as well as the current controllers are well designed.

Fig. 19 presents the stator current for phases a and b (i_a, i_b) for the same scenario of the previous result, but in a lower time scale. The stator current is a little distorted due to the relative low torque. As a result, the RMS value of the stator current is also low. Distortions in low RMS current are expected since harmonic components around the switching frequency have magnitudes close to the magnitude of the fundamental current component. By increasing the load torque, the fundamental current components increases while the switching frequency components keep unchanged. The result is a more clean stator current, as will be observer later.

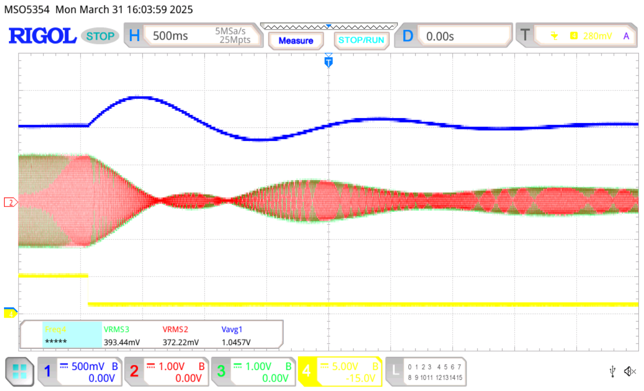

FIGURE 18. The electrical speed (ω) in channel 1, the stator current for phases a and b (i_a, i_b) in channels 2 and 3 and the mechanical load torque (T_L) in channel 4 for a transition of the load torque from 10 Nm to 2.5 Nm. Ch1:2000RPM/V Ch2:Ch3: 10A/V; Ch4: 2 Nm/V.

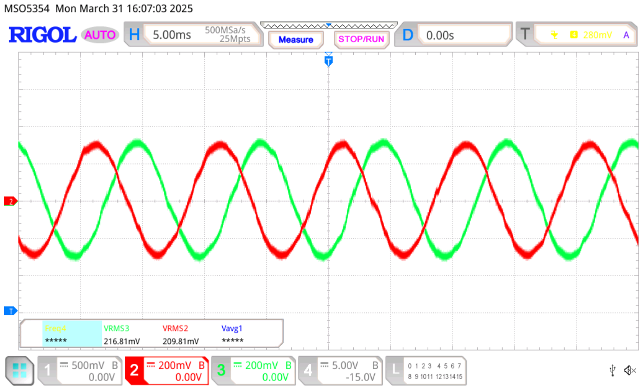

FIGURE 19. The stator current for phases a and b (i_a, i_b) in channels 2 and 3 for the same scenario of the previous result, but in a lower time scale. Ch2:Ch3: 10A/V.

Fig. 20 presents the electrical speed (ω), the stator current for phases a and b (i_a, i_b) and the mechanical load torque (T_L) for a transition at the speed reference from 2000 RPM to 1000 RPM. For this case, the load torque is kept constant at 10 Nm. This result shows also that the machine is correctly controlled also at 1000 RPM.

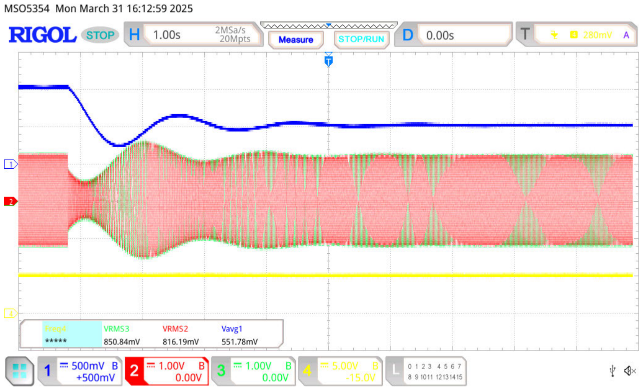

FIGURE 20. The electrical speed (ω) in channel 1, the stator current for phases a and b (i_a, i_b) in channels 2 and 3 and the mechanical load torque (T_L) in channel 4 for a transition at the speed reference from 2000 RPM to 1000 RPM. Ch1:2000RPM/V Ch2:Ch3: 10A/V; Ch4: 2 Nm/V.

Fig. 21 presents the stator current for phases a and b (i_a, i_b) for the same scenario of the previous result, but in a zoom visualization. Note that the stator current has actually cleaner sinusoidal waveform since the load torque is $10\,Nm$.

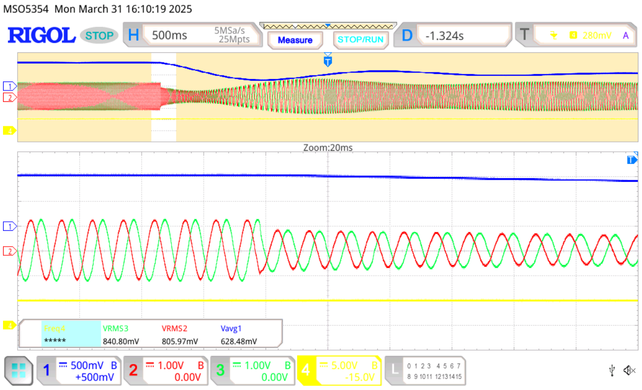

FIGURE 21. The stator current for phases a and b (i_a, i_b) in channels 1 and 2 for the same scenario of the previous result, but in zoom visualization. Ch1:2000RPM/V; Ch2:Ch3: 10A/V. Ch4: 2 Nm/V.

B. SECOND CASE

Tab. 3 shows the parameter of the second case evaluated on HIL and microcontroller [1]. The desired parameters are $\tau = 0.5\,ms$ and $f_c = 50\,Hz$. The designed parameters are also presented in this table.

The reason for choosing the same time constant and cut-off frequency for both Case I and Case II is to standardize the verification of the proposed control strategy and facilitate its evaluation. Since the machine parameters differ between Case I and Case II, using equal time constants and cut-off frequencies brings more legitimacy to the results, as different results for both cases show that the control is reacting according to the machine parameters, and not because they were designed differently. If different time constants and cut-off frequencies were chosen for Case I and Case II, it would be unclear whether the differences in results were due to the control strategy or the machine parameters. Therefore, to demonstrate that the proposed control strategy performs satisfactorily across different machine parameters, all control design specifications are kept consistent.

TABLE 4. System parameter for Case 2.

Parameters	Value	Parameters	Value
R_s	$1.2\,\Omega$	V_{dc}	$500\,V$
L_q	$12\,mH$	k_{pq}	24
L_d	$5.7\,mH$	k_{iq}	2400
P	4	k_{pd}	11.4
λ	$0.123\,Wb$	k_{id}	2400
J	$0.0005\,k_gm^2$	k_{ps}	2.349126
B	0.0001	k_{is}	23.491264
f_{sw}	$10\,kHz$		

Fig. 22 presents the electrical speed (ω), the stator current for phases a and b (i_a, i_b) and the electrical rotor position (θ) for steady-state operation. In this case, the reference speed is $2000\,RPM$ and the load torque is $2\,Nm$.

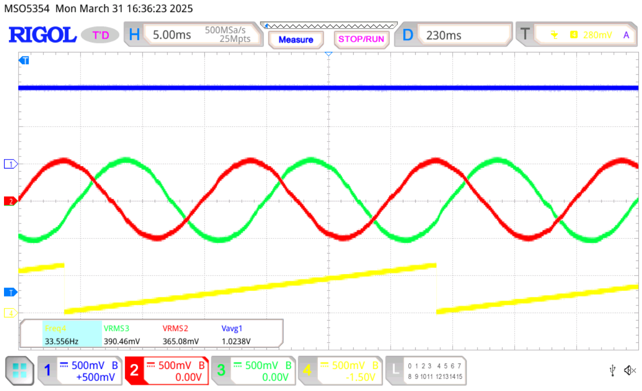

FIGURE 22. The electrical speed (ω) in channel 1, the stator current for phases a and b (i_a, i_b) in channel 2 and 3 and the electrical rotor position (θ) in channel 4 for steady-state operation. Ch1:2000RPM/V Ch2:Ch3: 10A/V; Ch4: 20 units/V.

Fig. 23 presents the electrical speed (ω), the stator current for phases a and b (i_a, i_b) and the mechanical load torque (T_L) for a transition of the load torque from $10\,Nm$ to $2.5\,Nm$. The electrical speed oscillates and returns to its nominal value after some seconds, indicating that speed controller as well as the current controllers are well designed.

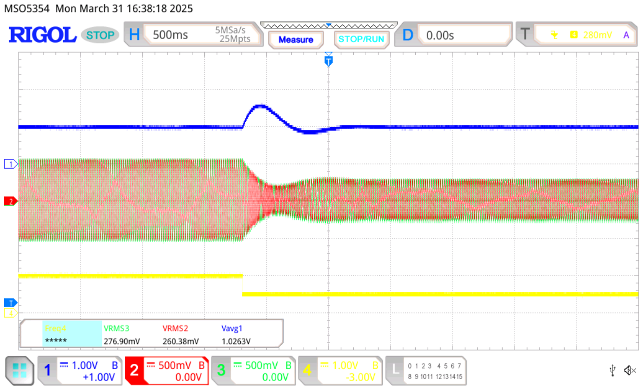

FIGURE 23. The electrical speed (ω) in channel 1, the stator current for phases a and b (i_a, i_b) in channels 2 and 3 and the mechanical load torque (T_L) in channel 4 for a transition of the load torque from 2 Nm to 1 Nm. Ch1:2000RPM/V Ch2:Ch3: 10A/V; Ch4: 2 Nm/V.

Fig. 24 presents the stator current for phases a and b (i_a, i_b) for the same scenario of the previous result, but in a lower time scale.

Fig. 25 presents the electrical speed (ω), the stator current for phases a and b (i_a, i_b) and the mechanical load torque (T_L) for a transition at the speed reference from $2000\,RPM$ to $1000\,RPM$. For this case, the load torque is kept constant at $2\,Nm$. A zoom in steady-state is also presented. This result shows also that the machine is correctly controlled also at $1000\,RPM$.

TABLE 5. Comparison of control strategies for interior PMSM.

Control Strategy	Principle of Working	Advantages	Disadvantages
Proposed FOC	Decouples torque and flux using d-q axis control.	Well-established, high efficiency, and smooth operation.	Requires accurate motor parameters; sensitive to variations.
DTC	Uses hysteresis controllers and switching tables for direct torque and flux control.	Fast torque response; no need for current controllers.	High torque and flux ripples; requires high switching frequency.
SMC	Uses sliding surfaces for robust nonlinear control.	Strong robustness against parameter variations and disturbances.	Chattering effect; difficult tuning.
MPC	Optimizes control inputs using a predictive model and cost function.	High-performance dynamic response; constraints handling.	Requires an accurate model; high computational burden.
MARS	Adapts control law based on real-time parameter estimation.	No need for an exact motor model; adaptive to changes.	Complex adaptation algorithms; sensitive to noise.
Deadbeat	Computes optimal control input to reach the desired state in one step.	Very fast response; reduced steady-state error.	Sensitive to noise and parameter variations.

Control Strategy	Computational Complexity	Dynamic Performance	Implementation Complexity
Proposed FOC	Moderate	Good	Moderate
DTC	Moderate to High	Very Fast	Moderate
SMC	High	Fast	High
MPC	Very High	Excellent	High
Model-less Adaptive (RLS)	High	Good	High
Deadbeat Control	High	Very Fast	Moderate to High

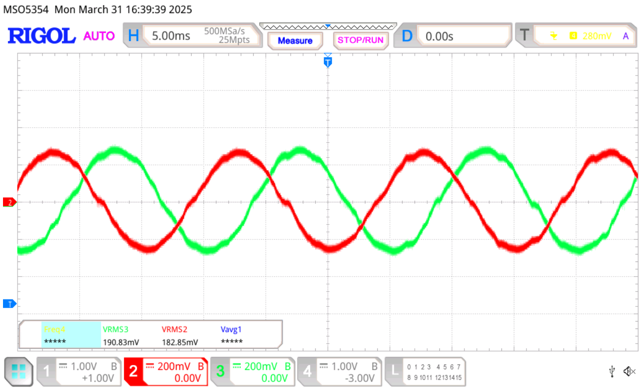

FIGURE 24. The stator current for phases a and b (i_a, i_b) in channels 2 and 3 for the same scenario of the previous result, but in a lower time scale. Ch2:Ch3: 10A/V.

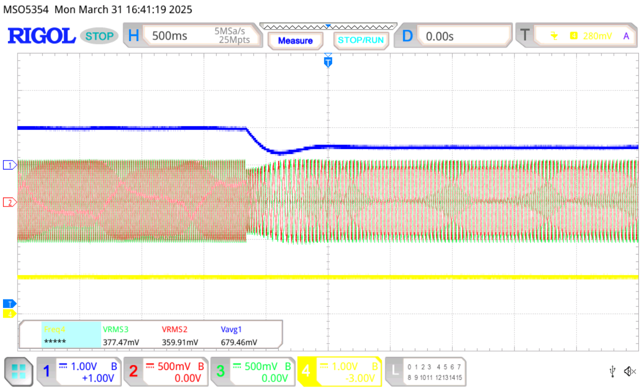

FIGURE 25. The electrical speed (ω) in channel 1, the stator current for phases a and b (i_a, i_b) in channels 2 and 3 and the mechanical load torque (T_L) in channel 4 for a transition at the speed reference from 2000 RPM to 1000 RPM. Ch1:2000RPM/V Ch2:Ch3: 10A/V; Ch4: 2 Nm/V.

Fig. 26 presents the stator current for phases a and b (i_a, i_b) for the same scenario of the previous result, but in a lower time scale.

VIII. COMPARISON OF CONTROL STRATEGIES FOR IPMSM

This section presents a comparison of various control strategies for IPMSM drives. The strategies covered include most of those discussed in the Introduction: the proposed FOC, DTC, SMC, MPC, MARS, and Deadbeat-based Control. These methods differ significantly in terms of computational complexity, control performance, and implementation efficiency.

Table 5 provides a comprehensive comparison of these control strategies, showing their working principles, benefits, and drawbacks. The proposed FOC remains one of the most attractive techniques, offering smooth operation but requiring precise motor parameters. DTC, on the other hand, ensures fast torque response but suffers from high torque and flux ripples. More advanced methods, such as MPC, enable excellent dynamic performance by predicting system behavior, but with a high computational costs. Meanwhile, adaptive control techniques like RLS-based methods offer flexibility by estimating parameters in real time, although its complex algorithm.

Selecting the most suitable control strategy depends on the specific application requirements, such as response time, robustness, and computational constraints. While FOC

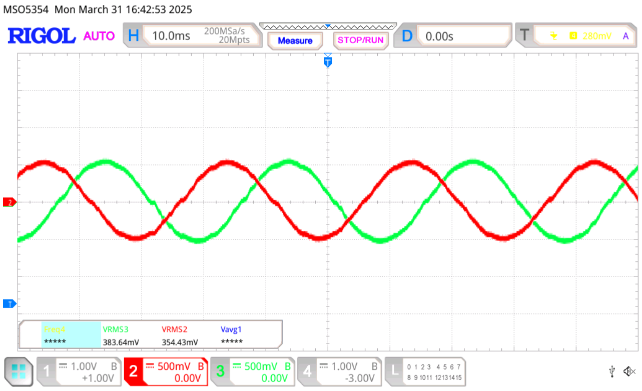

FIGURE 26. The stator current for phases a and b (i_a, i_b) in channels 2 and 3 for the same scenario of the previous result, but in a lower time scale. Ch2:Ch3: 10A/V.

and DTC remain practical choices for many industrial applications, MPC and adaptive control methods are gaining attention for high-performance and adaptive systems. Understanding these trade-offs is essential for designing efficient IPMSM control systems.

It is worth mentioning that robust controllers are also considered an attractive solution for PMSM drive systems. As presented in [51], an integral reinforcement learning-based H_∞ control algorithm for PMSM drives delivers excellent performance with guaranteed stability. Owing to its model-free nature, the proposed algorithm achieves superior current regulation without requiring prior knowledge of motor parameters. Another robust control approach is discussed in [52], which provides an overview of various robust control techniques for PMSMs, including the implementation of a speed controller. In light of uncertainty factors such as parameter perturbations and load disturbances, the paper primarily reviews H_∞ robust control strategies based on traditional techniques, such as robust H_∞ sliding mode control and H_∞ robust current control based on Hamilton–Jacobi Inequality theory.

IX. CONCLUSION

This paper proposes an comprehensive design approach for field-oriented control of Interior Permanent Magnet Synchronous Machines. The field-oriented control strategy was employed in the proposed approach. The electrical and mechanical models of the IPMSM were first introduced. Then, a detailed step-by-step procedure for tuning the current and speed controllers of the FOC strategy was presented. The speed controller was designed using the frequency response method. The analysis of parameter variations enabled a more accurate design of the FOC. A description of stability and the region of operation further contributed to the consistency of the controller.

Using the enhanced design approach, two case studies with different machines were performed. The entire system was tested in a Controller Hardware-in-the-Loop device with an external controller. Since the machine parameters differ between Case I and Case II, equal time constants and cut-off frequencies were adopted, bringing more legitimacy to the results, as different results for both cases show that the control is reacting according to the machine parameters, and not because they were designed differently. The results demonstrated the efficacy of the proposed design approach under steady-state conditions and during steps in the reference speed and mechanical load torque. The scripts and simulation files used in this research will be freely available on the author's webpage: https://busarello.prof.ufsc.br/.

APPENDIX

This Appendix presents the behavior of the controlled variables following their reference signals, the performance of the decoupling scheme and the superiority of the speed control designed based on the proposed method over a classical method.

The results of this section are from simulations. The reason for presenting only simulation results is that they involve variables that would run within the microcontroller, and collecting them in the experimental setup is unfeasible with the available lab resources.

Fig. 27 present dq-axis currents and their reference signals while At the top, it is shown the reference signal (id_{ref}) and the d-axis current while at the bottom we have the same variables, but for q-axis.

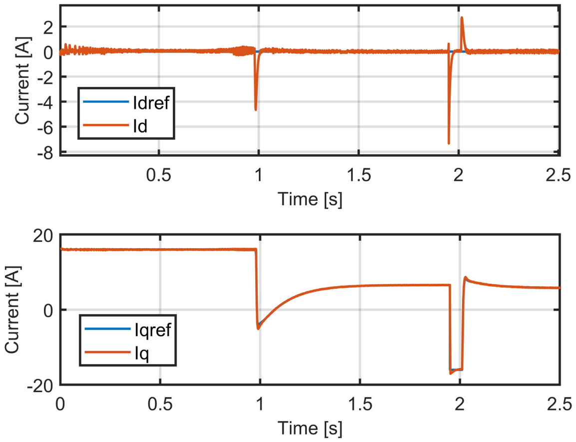

FIGURE 27. dq-axis currents and their reference signals.

Fig. 28 shows the d-axis reference and the d-axis current with and without the decoupling scheme. The d-axis reference is kept null, but the d-axis current passes through a transitory interval due to a reference change in the q-axis (not shown). With the decoupling scheme, it is possible to observe that the d-axis current presents lower overshoot, beyond the fact that the response is faster than the same current without employing any decoupling scheme. Note that eliminating completely the transitory in such a case is impractical because the PMSM modeling used as background for the decoupling scheme is done for steady-state conditions. Any models for transitory behavior would serve uniquely to a specific point of operation. The decoupling scheme adopted in this paper improves the transitory interval for all points of operation, but unfortunately does not eliminate it completely.

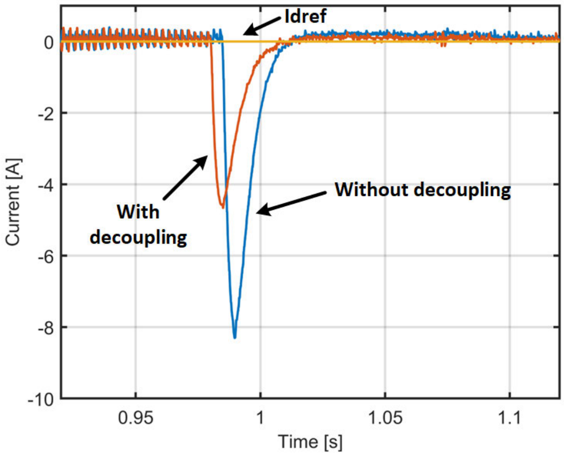

FIGURE 28. ***d*-axis reference and *d*-axis current with and without the decoupling scheme.**

Fig. 29 presents speed responses considering the speed control designed based on the proposed method and also based on a common method. These results were collected in a scenario of a step in the speed setpoint. The speed response considering the speed control designed based on a common method presents high overshoot. On the other hand, the response considering the proposed method presents lower overshoot, but high accommodation time. For machine applications, the last is more desirable. High overshoot in speed response means the PMSM runs at a considerable high speed compared to the speed setpoint, which may damage the mechanical parts coupled to the PMSM. The presented result is valid for a step-up change in the speed setpoint of the PMSM. Similar responses were observed during a step-down change.

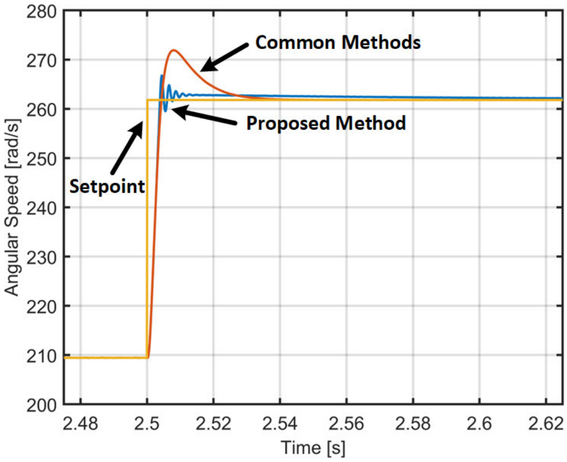

FIGURE 29. **Speed responses considering the speed control designed based on the proposed method and also based on a common method.**

REFERENCES

[1] R. Krishnan, *Permanent Magnet Synchronous and Brushless DC Motor Drives*. Boca Raton, FL, USA: CRC Press, Dec. 2017.

[2] E. Carfagna, C. M. Verrelli, G. Migliazza, F. Bernardi, and E. Lorenzani, "Stator flux observers for speed-controlled PMSMs in low-speed sensorless applications: Comparative tests and hybrid strategy," *IEEE Trans. Control Syst. Technol.*, early access, Feb. 6, 2025, doi: 10.1109/TCST.2025.3536203.

[3] S. Ye and X. Yao, "An enhanced SMO-based permanent-magnet synchronous machine sensorless drive scheme with current measurement error compensation," *IEEE J. Emerg. Sel. Topics Power Electron.*, vol. 9, no. 4, pp. 4407–4419, Aug. 2021.

[4] L. Gou, C. Wang, X. You, M. Zhou, and S. Dong, "IPMSM sensorless control for zero- and low-speed regions under low switching frequency condition based on fundamental model," *IEEE Trans. Transport. Electrific.*, vol. 8, no. 1, pp. 1182–1193, Mar. 2022.

[5] R. H. Arash Kiyoumarsi, *Interior Permanent-Magnet Synchronous Motors: Optimal Shape Design, Construction and Testing*. London, U.K.: LAP Lambert Academic, 2011.

[6] H. Yao, Y. Yan, T. Shi, G. Zhang, Z. Wang, and C. Xia, "A novel SVPWM scheme for field-oriented vector-controlled PMSM drive system fed by cascaded H-bridge inverter," *IEEE Trans. Power Electron.*, vol. 36, no. 8, pp. 8988–9000, Aug. 2021.

[7] M. Abassi, A. Khlaief, O. Saadaoui, A. Chaari, and M. Boussak, "Performance analysis of FOC and DTC for PMSM drives using SVPWM technique," in *Proc. 16th Int. Conf. Sci. Techn. Autom. Control Comput. Eng. (STA)*, Dec. 2015, pp. 228–233.

[8] C. Candelo-Zuluaga, J.-R. Riba, and A. Garcia, "PMSM parameter estimation for sensorless FOC based on differential power factor," *IEEE Trans. Instrum. Meas.*, vol. 70, pp. 1–12, 2021.

[9] F. Hilpert, C. Bentheimer, T. Mueller, and B. Eckardt, "Investigation of novel multi-phase field-oriented drive inverter control with fail-operational capabilities for aircraft applications," in *Proc. PCIM Eur. Digit. Days Int. Exhib. Conf. Power Electron., Intell. Motion, Renew. Energy Energy Manage.*, May 2021, pp. 1–7.

[10] A. Oprea and D. Floricau, "Field oriented control of permanent magnet synchronous motor with graphical user interface," in *Proc. 12th Int. Symp. Adv. Topics Electr. Eng. (ATEE)*, Mar. 2021, pp. 1–4.

[11] R. E. Quintal-Palomo, M. Flota-Bañuelos, A. Bassam, R. PEón-Escalante, F. Peñuñuri, and M. Dybkowski, "Post-fault demagnetization of a PMSG under field oriented control operation," *IEEE Access*, vol. 9, pp. 53838–53848, 2021.

[12] Z. Wang, J. Chen, M. Cheng, and K. T. Chau, "Field-oriented control and direct torque control for paralleled VSIs fed PMSM drives with variable switching frequencies," *IEEE Trans. Power Electron.*, vol. 31, no. 3, pp. 2417–2428, Mar. 2016.

[13] C. Zhang, X. Wang, D. Wang, Q. Sun, and G. Ma, "Comparative analysis of electromagnetic force inverter fed PMSM drive using field oriented control (FOC) and direct torque control (DTC)," in *Proc. 22nd Int. Conf. Electr. Mach. Syst. (ICEMS)*, Aug. 2019, pp. 1–4.

[14] H. A. G. Al-Kaf, S. S. Hakami, and K.-B. Lee, "Hybrid current controller for permanent-magnet synchronous motors using robust switching techniques," *IEEE Trans. Power Electron.*, vol. 38, no. 3, pp. 3711–3724, Mar. 2023.

[15] H. Ghanayem, M. Alathamneh, and R. M. Nelms, "Performance of a vector controlled PMSM drive based on proportional–resonance control under single-phase open circuit fault," *Energy Rep.*, vol. 9, pp. 755–763, Mar. 2023. [Online]. Available: https://www.sciencedirect.com/science/article/pii/S2352484722024994

[16] A. S. Bubshait, A. Mortezaei, M. G. Simões, and T. D. C. Busarello, "Power quality enhancement for a grid connected wind turbine energy system," *IEEE Trans. Ind. Appl.*, vol. 53, no. 3, pp. 2495–2505, May 2017.

[17] M. Nicola, C.-I. Nicola, D. Selişteanu, and C. Ionete, "Control of PMSM based on switched systems and field-oriented control strategy," *Automation*, vol. 3, no. 4, pp. 646–673, Dec. 2022. [Online]. Available: https://www.mdpi.com/2673-4052/3/4/33

[18] J. You, M. Yang, C. Shang, P. Shan, and D. Xu, "A high controller parameters robust decoupling based on complex vector for permanent magnet synchronous motor," in *Proc. 25th Int. Conf. Electr. Mach. Syst. (ICEMS)*, Nov. 2022, pp. 1–6.

[19] A. Huang, Z. Chen, and J. Wang, "Research on the dq-axis current reaction time of an interior permanent magnet synchronous motor for electric vehicle," *World Electric Vehicle J.*, vol. 14, no. 7, p. 196, Jul. 2023.

[20] P. Stumpf and T. Tóth-Katona, "Recent achievements in the control of interior permanent-magnet synchronous machine drives: A comprehensive overview of the state of the art," *Energies*, vol. 16, no. 13, p. 5103, Jul. 2023.

[21] J. Liu, C. Gong, Z. Han, and H. Yu, "IPMSM model predictive control in flux-weakening operation using an improved algorithm," *IEEE Trans. Ind. Electron.*, vol. 65, no. 12, pp. 9378–9387, Dec. 2018.

[22] S. A. Odhano, P. Pescetto, H. A. A. Awan, M. Hinkkanen, G. Pellegrino, and R. Bojoi, "Parameter identification and self-commissioning in AC motor drives: A technology status review," *IEEE Trans. Power Electron.*, vol. 34, no. 4, pp. 3603–3614, Apr. 2019.

[23] R. Thakkar, H. Bhatt, and D. Dalwadi, "Review on different algorithm of interior permanent magnet synchronous motor (IPMSM)," in *Proc. IEEE India Council Int. Subsections Conf. (INDISCON)*, Jul. 2022, pp. 1–6.

[24] A. Khlaief, M. Bendjedia, M. Boussak, and M. Gossa, "A nonlinear observer for high-performance sensorless speed control of IPMSM drive," *IEEE Trans. Power Electron.*, vol. 27, no. 6, pp. 3028–3040, Jun. 2012.

[25] E.-K. Kim, J. Kim, H. H. Choi, and J.-W. Jung, "Variable structure speed controller guaranteeing robust transient performance of an IPMSM drive," *IEEE Trans. Ind. Informat.*, vol. 15, no. 6, pp. 3300–3310, Jun. 2019.

[26] B. Ding, Y. Lu, C. Lai, and G. Feng, "Single open-phase fault tolerant control of salient dual three-phase PMSMs with maximized torque to total loss ratio considering peak phase current limit," *IEEE Trans. Ind. Electron.*, early access, Jan. 1, 2025, doi: 10.1109/TIE.2024.3519589.

[27] J. Yang, W.-H. Chen, S. Li, L. Guo, and Y. Yan, "Disturbance/uncertainty estimation and attenuation techniques in PMSM drives—A survey," *IEEE Trans. Ind. Electron.*, vol. 64, no. 4, pp. 3273–3285, Apr. 2017.

[28] S. Li, B. Sarlioglu, S. Jurkovic, N. R. Patel, and P. Savagian, "Analysis of temperature effects on performance of interior permanent magnet machines for high variable temperature applications," *IEEE Trans. Ind. Appl.*, vol. 53, no. 5, pp. 4923–4933, Sep. 2017.

[29] C. Zhang, G. Wu, F. Rong, J. Feng, L. Jia, J. He, and S. Huang, "Robust fault-tolerant predictive current control for permanent magnet synchronous motors considering demagnetization fault," *IEEE Trans. Ind. Electron.*, vol. 65, no. 7, pp. 5324–5334, Jul. 2018.

[30] C. Lai, G. Feng, K. Mukherjee, and N. C. Kar, "Investigations of the influence of PMSM parameter variations in optimal stator current design for torque ripple minimization," *IEEE Trans. Energy Convers.*, vol. 32, no. 3, pp. 1052–1062, Sep. 2017.

[31] H. Wang, C. Gan, C. Zhang, H. Ren, and R. Qu, "Parameter robust predictive current control for PMSM drives based on self-tuning incremental model and voltage constraint compensation," *IEEE Trans. Power Electron.*, early access, Feb. 10, 2025, doi: 10.1109/TPEL.2025.3539434.

[32] A. Brosch, O. Wallscheid, and J. Böcker, "Model predictive control of permanent magnet synchronous motors in the overmodulation region including six-step operation," *IEEE Open J. Ind. Appl.*, vol. 2, pp. 47–63, 2021.

[33] B. Guo, S. Bacha, and M. Alamir, "A review on ADRC based PMSM control designs," in *Proc. 43rd Annu. Conf. IEEE Ind. Electron. Soc. (IECON)*, Oct. 2017, pp. 1747–1753.

[34] S.-K. Kim, J.-S. Lee, and K.-B. Lee, "Self-tuning adaptive speed controller for permanent magnet synchronous motor," *IEEE Trans. Power Electron.*, vol. 32, no. 2, pp. 1493–1506, Feb. 2017.

[35] R. Cai, R. Zheng, M. Liu, and M. Li, "Robust control of PMSM using geometric model reduction and μ-synthesis," in *Proc. 42nd Annu. Conf. IEEE Ind. Electron. Soc. (IECON)*, Oct. 2016, pp. 2885–2891.

[36] E. Brescia, M. Tipaldi, F. Torelli, P. R. Massenio, L. P. Savastio, G. L. Cascella, and E. De Tuglie, "A continuous sliding mode current control based on the sensitivity theory for PMSM drives," *IEEE Open J. Ind. Appl.*, vol. 6, pp. 48–58, 2025.

[37] Y. He, Z. Cao, J. Mao, K. Liang, and C. Zhang, "Adaptive super-twisting sliding mode control with disturbance compensation for speed regulation of PMSM system," *IEEE Control Syst. Lett.*, vol. 8, pp. 3410–3415, 2024.

[38] J. Xu, T. B. Soeiro, Y. Wang, Y. Wu, H. Tang, and P. Bauer, "A novel voltage reconstruction method for MRAS based sensorless IPMSM drives," in *Proc. IEEE 19th Int. Power Electron. Motion Control Conf. (PEMC)*, Apr. 2021, pp. 225–230.

[39] F.-J. Lin, S.-Y. Chen, I.-M. Hsu, and C.-X. Xu, "Robust deadbeat predict current control using intelligent integral sliding mode control for interior permanent magnet synchronous motor drive," *IEEE Trans. Transport. Electric.*, early access, Feb. 6, 2025, doi: 10.1109/TTE.2025.3539298.

[40] J. Wu, J. Wang, C. Gan, Q. Sun, and W. Kong, "Efficiency optimization of PMSM drives using field-circuit coupled FEM for EV/HEV applications," *IEEE Access*, vol. 6, pp. 15192–15201, 2018.

[41] T. D. C. Busarello, A. Bubshait, O. V. S. R. Varaprasad, A. Alsaleem, and M. G. Simões, "Comprehensive design approach for field-oriented control of interior permanent magnet synchronous machines," in *Proc. 4th Global Power, Energy Commun. Conf. (GPECOM)*, Jun. 2022, pp. 168–173.

[42] T. D. C. Busarello, "Contributions to discrete-time sliding mode observers for permanent magnet synchronous motor drive systems," in *Proc. 4th Global Power, Energy Commun. Conf. (GPECOM)*, Jun. 2022, pp. 162–167.

[43] Z. Li, G. Feng, C. Lai, D. Banerjee, W. Li, and N. C. Kar, "Current injection-based multi-parameter estimation for dual three-phase IPMSM considering VSI nonlinearity," *IEEE Trans. Transport. Electrific.*, vol. 5, no. 2, pp. 405–415, Jun. 2019.

[44] M. S. Rafaq and J.-W. Jung, "A comprehensive review of state-of-the-art parameter estimation techniques for permanent magnet synchronous motors in wide speed range," *IEEE Trans. Ind. Informat.*, vol. 16, no. 7, pp. 4747–4758, Jul. 2020.

[45] K. Lee, J.-I. Ha, and D. V. Simili, "Analysis and suppression of slotting and cross-coupling effects on current control in PM synchronous motor drives," *IEEE Trans. Power Electron.*, vol. 34, no. 10, pp. 9942–9956, Oct. 2019.

[46] Z. Q. Zhu, D. Liang, and K. Liu, "Online parameter estimation for permanent magnet synchronous machines: An overview," *IEEE Access*, vol. 9, pp. 59059–59084, 2021.

[47] H. Cheng, M. S. Toulabi, U. Deshpande, and N. C. Kar, "Multiparameter estimation of IPMSMs using core loss current calculations in dq-axis equivalent circuit model," *IEEE Trans. Ind. Appl.*, vol. 59, no. 2, pp. 1295–1306, Mar. 2023.

[48] Z. Chen, S. Jin, Y. Shen, and M. Wang, "Loss minimum control of surface permanent magnet synchronous motor based on virtual complementary square wave signal injection," *IEEE J. Emerg. Sel. Topics Power Electron.*, early access, Feb. 4, 2025, doi: 10.1109/JESTPE.2025.3538598.

[49] Z. Fangyang, R. Feng, L. Jianjun, and H. Peng, "Study on flux-weakening control for PMSM," in *Proc. 4th Int. Symp. Knowl. Acquisition Modeling*, Oct. 2011, pp. 192–195.

[50] S. Morimoto, M. Sanada, and Y. Takeda, "Wide-speed operation of interior permanent magnet synchronous motors with high-performance current regulator," *IEEE Trans. Ind. Appl.*, vol. 30, no. 4, pp. 920–926, Apr. 1994.

[51] Q. Guan, X. Yao, Z. Lin, J. Wang, H. Ho Ching Iu, T. Fernando, and X. Zhang, "A robust control scheme for PMSM based on integral reinforcement learning," *IEEE Trans. Transport. Electric.*, vol. 11, no. 1, pp. 4214–4223, Feb. 2025.

[52] K. Ullah, J. Guzinski, and A. F. Mirza, "Critical review on robust speed control techniques for permanent magnet synchronous motor (PMSM) speed regulation," *Energies*, vol. 15, no. 3, p. 1235, Feb. 2022.

TIAGO DAVI CURI BUSARELLO (Senior Member, IEEE) received the bachelor's degree in electrical engineering from the State University of Santa Catarina, in 2010, and the master's and Ph.D. degrees in electrical engineering from the State University of Campinas (UNICAMP), Brazil, in 2013 and 2015, respectively. He has been a Professor with the Federal University of Santa Catarina (UFSC), Brazil, since 2016. He was a Postdoctoral Researcher with the University of Vaasa, Finland, from 2022 to 2023; and a Visiting Researcher with Colorado School of Mines, USA, in 2014. He is the author of the books *Power Electronic Converters and Systems* (Volumes 1 and 2, both published by IET, in 2024). He has also contributed chapters to several other technical books. His research interests include digital control for power electronics, digital twins, and power quality. He is a member of the IEEE Power Electronics Society.

ABDULLAH BUBSHAIT received the B.Sc. degree in electrical engineering from the King Fahd University of Petroleum and Minerals (KFUPM), Saudi Arabia, in 2005, the M.Sc. degree in electrical engineering from the University of Calgary, Canada, in 2011, and the Ph.D. degree from Colorado School of Mines, in 2018. Currently, he is an Assistant Professor with the Department of Electrical Engineering, King Faisal University, Saudi Arabia. His research interests include design, control, and modeling of grid-forming and grid-following inverters; and integration of renewable energy resources into power grid and power quality.

ORUGANTI V. S. R. VARAPRASAD (Member, IEEE) received the Ph.D. degree in electrical engineering from the National Institute of Technology Warangal, India, in 2019. He has 12 years of teaching and research experience. He is currently a Postdoctoral Fellow with the Smart Transportation Electrification and Energy Research (STEER) Group, Department of Electrical, Computer, and Software Engineering, Faculty of Engineering and Applied Science, Ontario Tech University, Oshawa, ON, Canada. He was a Visiting Scholar with Colorado School of Mines, USA, under the prestigious BHASKARA Advanced Solar Energy Fellowship, in 2015, awarded by Indo-U.S. Science and Technology Forum (IUSSTF) and the Department of Science and Technology (DST), Government of India. His current research focuses on advanced power electronic converters for electric vehicle (EV) charging applications, multifunctional inverters, cybersecurity, and power quality. He is a Life Member of Indian Society for Technical Education; and an Active Member of the IEEE Power Electronics Society, the IEEE Power and Energy Society, the IEEE Industrial Applications Society, and the IEEE Industrial Electronics Society. He received the POSOCO Power System Award, in 2017, for the Ph.D. work, jointly presented by Power System Operation Corporation Ltd. (POSOCO), a Government of India enterprise, and the Foundation for Innovation and Technology Transfer (FITT); and the Postdoctoral Fellow Excellence Award from Ontario Tech University, in 2025.

ABDULHAKEEM ALSALEEM received the Ph.D. degree in electrical engineering from Colorado School of Mines, USA, in 2020. He is currently an Assistant Professor with the Department of Electrical Engineering, College of Engineering, Qassim University, Saudi Arabia. His research interests include power electronics, with a particular focus on dc–dc converters, modeling, control, and magnetics design for power electronic systems.

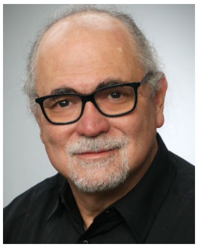

MARCELO GODOY SIMÕES (Fellow, IEEE) received the B.Sc. and M.Sc. degrees from the University of São Paulo, Brazil, in 1985 and 1990, respectively, the Ph.D. degree from The University of Tennessee, USA, in 1995, and the D.Sc. degree (Livre-Docancia) from the University of São Paulo, in 1998. He has been with the University of Vaasa, Finland, since 2021, as a Professor in flexible and smart power systems. He is a pioneer to apply neural networks and fuzzy logic in power electronics, motor drives, and renewable energy systems. His fuzzy logic-based modeling and control for wind turbine optimization is used as a basis for advanced wind turbine control and it has been cited worldwide. His leadership in modeling fuel cells is internationally and highly influential in providing a basis for further developments in fuel cell automation control in many engineering applications. He has made substantial and lasting contribution of artificial intelligence technology in many applications, power electronics and motor drives, fuzzy control of wind generation systems, such as fuzzy logic-based waveform estimation for power quality, neural network-based estimation for vector-controlled motor drives and integration of alternative energy systems to the electric grid through AI modeling-based power electronics control. His current research interests include power electronics, power systems, power quality, smart-grids, and renewable energy systems. He was an U.S. Fulbright Fellow of AY 2014–2015, working for Aalborg University, Institute of Energy Technology, Denmark. He was elevated to the grade of IEEE Fellow, with the citation: “for applications of artificial intelligence in control of power electronics systems.”

• • •